Four-dimensional Langevin approach to fission with Cassini shape parameterization

Kazuki Okada[1,*], *Takahiro* Wada[1,**], and *Nicolae* Carjan[2,3,***]

[1]Department of Pure and Applied Physics, Kansai University, 564-8680 Suita, Osaka, Japan
[2]Joint Institute for Nuclear Research, 141980 Dubna, Moscow Region, Russia
[3]*Horia Hulubei* - National Institute for Nuclear Physics and Engineering, P.O.Box MG-6, RO-76900, Bucharest, Romania

Abstract. We apply the Cassini shape parameterization to the dynamical study of actinide fission using the multi-dimensional Langevin equation. The fragment mass distributions for fission of ^{236}U and ^{256,258}Fm are calculated with the 4D Langevin equation. The 4D collective space is formed by adding either α_3 or α_6 to the basic 3D $\{\alpha, \alpha_1, \alpha_4\}$ space. We investigate the role of α_3 and α_6 by comparing the results of 4D (α_3 or α_6) with that of 3D. For ^{236}U and ^{256}Fm, where asymmetric fission is predominant, the fragment mass distributions calculated in the 4D (α_3) space are in good agreement with experimental data. On the other hand, for ^{258}Fm, which is characterized by symmetric fission, 4D (α_6) is effective for describing the shape of compact symmetric fragments. We demonstrate the advantages of the Cassini shape parameterization for the dynamical study of actinide fission.

1 Introduction

The dynamical approach using the multi-dimensional Langevin equation is widely accepted as a practical method in the study of nuclear fission [1, 2]. In this approach, the nuclear shape is represented by a shape parameterization; a set of deformation parameters such as elongation, mass asymmetry and neck radius. The fission process is described by the multi-dimensional Langevin equation as the time evolution of the deformation parameters. Since this is not a self-consistent calculation, the choice of the shape parameterization determines the model space and the results of the Langevin calculation are largely dependent on it. Therefore, it is important to select the shape parameterization, where a small number of deformation parameters covers a variety of deformed nuclear shapes relevant to the fission process.

The original Cassini ovals are suitable for describing shapes of fissioning nuclei because they can draw spherical, elongated, and even two separated objects depending on the elongation parameter α. To allow more flexibility, Pashkevich proposed the generalized Cassini ovals, in which the surface is defined by a Legendre expansion [3]. Here, the deformation parameters are the coefficients α_n of the n-th order Legendre polynomial. The potential energies of deformation for ^{208}Pb, ^{230}Th, ^{236}U, ^{240}Pu, ^{252}Cf were calculated by the macroscopic-microscopic approach in the (α, α_1) plane [3]. In particular, macroscopic energy and shell and pairing correction of ^{236}U around scission were analyzed in detail [4]. Later, by considering statistical equilibrium in the deformation space, Carjan *et al.* established a method to calculate the fragment mass and total kinetic energy distributions from the potential and computed them for Fm to Rf [5]. Recently, they reported the fragment mass and total kinetic energy distributions in the super-heavy nuclear region [6, 7]. They have shown in these studies that not only α_1 but also α_3, α_4 and α_6 are essential parameters for describing the fragment shapes. However, these are calculated with the elongation parameter α fixed at scission, and the dynamical effects are neglected. As a next step, it is definitely important to use the Cassini shape parameterization in the framework of the Langevin equation and to calculate the time evolution of $\{\alpha, \alpha_n\}$ from the ground state to scission.

In the present paper, we will demonstrate the effectiveness of the Cassini shape parameterization by solving the four-dimensional (4D) Langevin equation. We will use $\{\alpha, \alpha_1, \alpha_3, \alpha_4\}$ or $\{\alpha, \alpha_1, \alpha_4, \alpha_6\}$ as a collective space. We will further investigate the role of α_3 and α_6 in the description of fragment shapes by comparing the fragment mass distributions and the average scission shapes between 3D $\{\alpha, \alpha_1, \alpha_4\}$ and 4D (3D + α_3 or α_6). In Sect. 2, we will describe the Cassini shape parameterization and the multi-dimensional Langevin equation. In Sect. 3, we will show the calculation results for neutron-induced fission of U and spontaneous fission of Fm. In Sect. 4, we will give the summary.

2 Formalism

2.1 Cassini shape parameterization

In the Cassini shape parameterization [3], the lemniscate coordinate (R, x) is used as an orthogonal system to de-

*e-mail: k319244@kansai-u.ac.jp
**e-mail: wadataka@kansai-u.ac.jp
***e-mail: carjan@cenbg.in2p3.fr

scribe nuclear shapes. The $R = const$ lines correspond to the surface of Cassini ovals which represents the division of a spherical shape into separated objects by varying the elongation parameter α. The original Cassini oval at $\alpha = 0$ shows the spherical shape, and $\alpha = 1$ shows a zero-neck configuration. Thus, α is considered as the main fission coordinate.

To include various deformations into the original Cassini ovals, the Legendre expansion of the surface is introduced by

$$R(x) = R_0 \left[1 + \sum_n \alpha_n P_n(x) \right], \quad (1)$$

where R_0 is the radius of the spherical nucleus and $P_n(x)$ is the Legendre polynomials. α_n are considered as the deformation parameters in the Cassini shape parameterization. In particular, α_1 and α_4 are important parameters that should be incorporated in calculations for any system because α_1 directly corresponds to the mass asymmetry of fragments at scission and α_4 is necessary for describing the symmetric deformation such as the ground state, the 1st barrier and the 2nd minimum. $\{\alpha, \alpha_1, \alpha_4\}$ is the standard 3D parameter set.

In this study, we focus on α_3 and α_6 as the fourth parameter. In the following, we show the role of α_3 and α_6 in describing important shapes in the fission process. Figure 1 shows typical shapes that can be described by the Cassini shape parameterization. The top left figure is drawn using only α_1 and shows that both fragments have similar deformations. On the other hand, the bottom left figure shows a nearly spherical fragment and a largely deformed fragment, depicted using only α_3. Thus, α_3 can represent the shape-asymmetric deformation. In the 4D calculation the mass-asymmetry is determined by the combination of α_1 and α_3. α_6 corresponds to the octupole deformation of fragments and is related to the distance between the centers of mass of the fragments. As shown in two figures on the right side of Fig. 1, α_6 can describe outwardly elongated or compact shapes depending on the sign. We expect that α_6 is necessary to describe the shapes corresponding to the super-long and super-short symmetric fission.

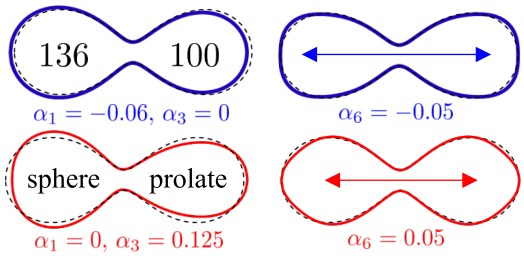

Figure 1: Dependence of the Cassini ovals on α_1, α_3 (left) and α_6 (right) at scission $\alpha = 0.985$. In each figure, a dotted line shows a shape with $\alpha_n = 0$.

2.2 Multi-dimensional Langevin equation

The multi-dimensional Langevin equations for describing the time evolution of collective coordinate q_i and conjugate momentum p_i of q_i are given as

$$\frac{dq_i}{dt} = m_{ij}^{-1} p_j$$
$$\frac{dp_i}{dt} = -\gamma_{ij} m_{jk}^{-1} p_k - \frac{\partial V}{\partial q_i} - \frac{1}{2} \frac{\partial m_{jk}^{-1}}{\partial q_i} p_j p_k + g_{ij} R(2)$$

where V is the potential energy of deformation, m_{ij} is the macroscopic inertia tensor from [8], and γ_{ij} is the macroscopic friction tensor from [9]. The potential energy of deformation is computed with the microscopic-macroscopic method [10] and includes the damping effect of the microscopic potential [11]:

$$V(\boldsymbol{q}, T) = V_{\mathrm{FRLDM}}(\boldsymbol{q}) + V_{\mathrm{micro}}(\boldsymbol{q}) \exp(-aT^2/E_d), \quad (3)$$

where a is the constant level density parameter taken from [12], the damping factor $E_D = 25$ MeV is used in this study and T is the nuclear temperature computed with $T = \sqrt{E_{\mathrm{int}}/a}$ based on the Fermi gas model. The internal energy E_{int} is calculated by the condition of the total energy conservation at each time step of the Langevin calculation.

g_{ij} is determined by the Einstein relation $T^* \gamma_{ij} = g_{ik} g_{kj}$, where T^* is effective nuclear temperature [13]. It is related to T by $T^* = (\hbar\omega/2) \coth(\hbar\omega/2T)$ with $\hbar\omega = 1.2$ MeV. The random number R_j is characterized by the white noise with $\langle R_i(t) \rangle = 0$ and $\langle R_i(t) R_j(t') \rangle = 2\delta_{ij}\delta(t-t')$ where $\langle\rangle$ denotes average over an ensemble.

3 Numerical results

We approach to fission by solving the 3D Langevin equation with a standard parameter set $\{\alpha, \alpha_1, \alpha_4\}$. We also perform the 4D Langevin calculation with additional parameters α_3 and α_6. In order to obtain the fragment mass distributions with a sufficient accuracy, we simulate the fission process for two million nuclei at the ground state until a half of them reach the scission condition $\alpha = 0.985$.

3.1 Neutron-induced fission of ^{235}U

In this section, we focus on the neutron-induced fission of ^{235}U. It is well known that the fragment mass distribution of U has a characteristic of asymmetric fission. The combination of fragments consists of a spherical nucleus and the remaining nucleus with deformation, because the double magic nucleus ^{132}Sn shows strong stability when it is spherical. In the calculation using Cassini shape parameterization, α_3 is expected to play an important role. Therefore, we compare the results of the fragment mass distributions in two deformation spaces: 3D $\{\alpha, \alpha_1, \alpha_4\}$ and 4D $\{\alpha, \alpha_1, \alpha_3, \alpha_4\}$. We consider that the two cases of incident neutron energy: thermal (almost 0 MeV) and 14 MeV.

Figure 2 shows the fragment mass distributions of thermal and 14 MeV neutron-induced fission calculated with the 3D and 4D Langevin equations. The experimental values are also shown [14, 15]. As can be seen, all distributions indicate that asymmetric fission is dominant; especially the distributions for the thermal neutron-induced

fission shows almost no symmetric component. Compared with the experimental data, the 3D results show that the peak position is found to be too mass asymmetric and the distribution is narrower. On the other hand, it is found that the 4D calculation with the addition of α_3 gives distributions with the peak position shifted to mass symmetric division in better agreement with the experimental data than the 3D results.

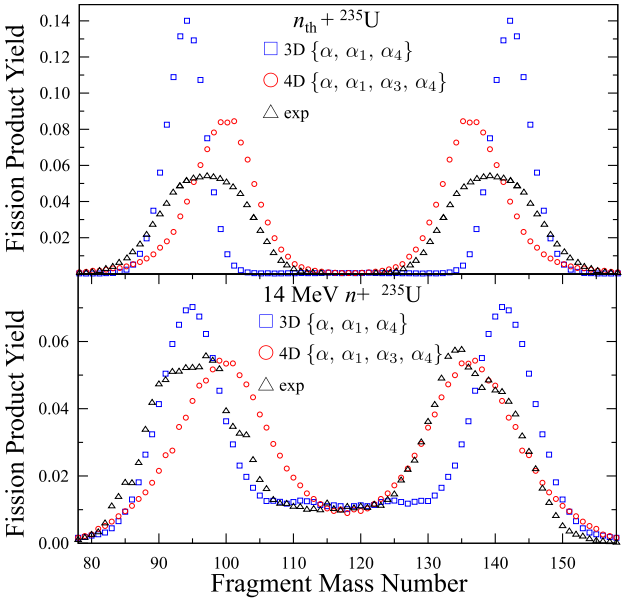

Figure 2: Fragment mass distributions for thermal (top) and 14 MeV (bottom) neutron-induced fission of ^{235}U. Squares give the result of 3D $\{\alpha, \alpha_1, \alpha_4\}$ and circles give that of 4D $\{\alpha, \alpha_1, \alpha_3, \alpha_4\}$. Triangles show the experimental data of thermal [14] and 14 MeV [15] neutron-induced fission of ^{235}U.

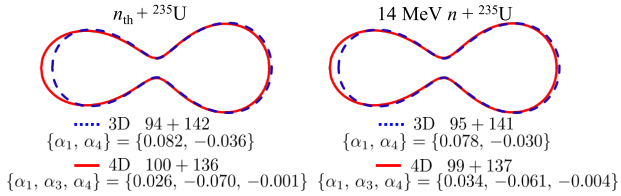

Figure 3: Average scission shapes of fragments corresponding to the peak positions of their mass distributions for thermal (left) and 14 MeV (right) neutron-induced fission of ^{235}U in Fig. 2. A Dash line gives the result of 3D $\{\alpha, \alpha_1, \alpha_4\}$ and a solid line gives that of 4D $\{\alpha, \alpha_1, \alpha_3, \alpha_4\}$. The bottom of the illustrations show the average values of the Cassini parameters and the combinations of fragment masses. α = 0.985.

To demonstrate the role of α_3 to the fragment shape, we pick out the trajectories of asymmetric fission from the events that reached scission and calculate the average values of the Cassini parameters at scission. We show in Fig. 3 the average shapes for thermal and 14 MeV neutron-induced fission of ^{235}U. The average shape is described using the average value of the Cassini parameters at scission, which indicates fragment masses corresponding to the peak position of the distribution in Fig. 2. The fragment masses and the average values of the Cassini parameters are listed below the average shapes. The 3D results show that the average shapes consist of two fragments with similar deformations. On the other hand, 4D results show that the heavy fragment is almost spherical and the light fragment is prolate. The difference between 3D and 4D can be understood to be due to the fact that α_3 describes the shape asymmetry of the fragments, which strongly reflects the shell effect of ^{132}Sn. Therefore, we can conclude that the shape asymmetry of fragments α_3 is an effective parameter when dealing with asymmetric fission.

3.2 Spontaneous fission of ^{256}Fm and ^{258}Fm

As another example of actinide nuclei, we examine spontaneous fission of Fm isotopes. In this element, it is known that the fragment mass distribution in spontaneous fission changes dramatically with neutron number, being asymmetric at N=156 and symmetric at N=158 [15, 16]. To investigate the effectiveness of the Cassini shape parameterization, we calculate the fission process of ^{256}Fm and ^{258}Fm at low excitation energy.

Figure 4 shows the fragment mass distributions for the fission of ^{256}Fm and ^{258}Fm. At the beginning, we focus on the distributions obtained using 3D and 4D (3D + α_3). In the ^{256}Fm results, as in ^{236}U, the addition of α_3 moves the peak position of the distribution inward and reproduces the experimental data well. On the other hand, in ^{258}Fm, the peak of the distribution at symmetric separation is eliminated by the addition of α_3. As a result, it is completely different from the experimental data.

Since ^{258}Fm is characterized by symmetric fission, α_6 is expected to play an important role in improving the fragment mass distribution. We solve the Langevin equation in 4D $\{\alpha, \alpha_1, \alpha_4, \alpha_6\}$ space using α_6 instead of α_3. The results are shown by the triangles in Fig. 4. The distribution of ^{258}Fm shows that the peak at asymmetric fission is lower than that of 3D and symmetric fission is dominant. It is found that the distribution of ^{258}Fm is in better agreement with experimental data. On the other hand, the ^{256}Fm result shows the same trend as the ^{258}Fm one when α_6 is added, which is not consistent with the experimental data. Therefore, α_6 is considered to be effective in treating systems characterized by symmetric fission.

To investigate the contribution of the additional parameters α_3 and α_6 to the fragment shapes, we focus on the average shapes of fragments. For ^{256}Fm, the average shape by 4D in Fig. 5 indicates the deformation of shape asymmetry. As in ^{236}U, α_3 is important for the description of asymmetric deformation. For the 4D averaged shape of ^{258}Fm, we use α_6 instead of α_3 and fix the mass number of fragments at 129, corresponding to symmetric fission. As can be seen, the shape is more compact in 4D. The distance between the centers of masses calculated from the Cassini parameters in Fig. 5 is $2.34R_0$ in 3D and $2.15R_0$ in 4D. This suggests that α_6 can describe the super-short symmetric fission. We assume that this effect is essential in discussing symmetric fission.

From the discussion with the results of ^{256}Fm and ^{258}Fm, it is found that α_3 and α_6 are important for describing the fragment shapes. In this study, we treat α_3 and α_6 separately, but it is desirable to use both α_3 and α_6 for the fission of ^{256}Fm and ^{258}Fm consistently. We will do this in the next study.

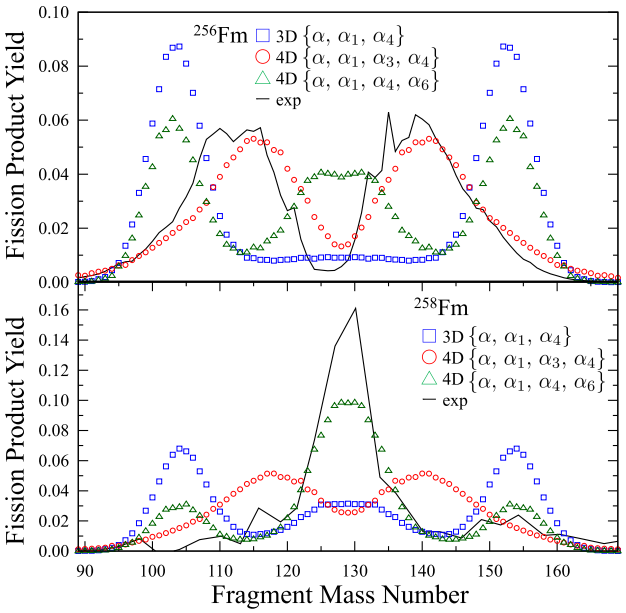

Figure 4: The same as in Fig. 2 but changed to ^{256}Fm (top) and ^{258}Fm (bottom) and included the results of 4D $\{\alpha, \alpha_1, \alpha_4, \alpha_6\}$. Solid line shows the experimental data of ^{256}Fm from [15] and of ^{258}Fm from [16].

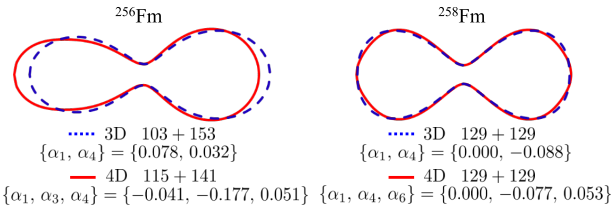

Figure 5: The same as in Fig. 3, but for ^{256}Fm (left) and ^{258}Fm (right). For ^{258}Fm, the result of 4D $\{\alpha, \alpha_1, \alpha_4, \alpha_6\}$ is used instead of 4D $\{\alpha, \alpha_1, \alpha_3, \alpha_4\}$.

4 Summary

We apply the Cassini shape parameters to the Langevin equation, which can describe various shapes of fission fragments. We obtain the fragment mass distribution by solving the 3D Langevin equation with $\{\alpha, \alpha_1, \alpha_4\}$ as the standard parameter set and the 4D Langevin equation with α_3 and α_6 added to 3D. Results are given for thermal and 14 MeV neutron-induced fission of ^{235}U. In the distribution of 4D $\{\alpha, \alpha_1, \alpha_3, \alpha_4\}$, the mass-asymmetry at the peak position is inside the 3D, which better reproduces the experimental data. From the analysis of the shapes of fission fragments, it is found that α_3 represents the shape asymmetry of fragments and is important to reflect the shell effect of ^{132}Sn. We also present results for the spontaneous fission of Fm isotopes. For ^{256}Fm, which is characterized by asymmetric fission, α_3 is important for describing the fragment shapes. On the other hand, for ^{258}Fm, which is characterized by symmetric fission, α_6 is appropriate instead of α_3. In conclusion, the five Cassini parameters α, α_1, α_3, α_4 and α_6 are important in the Langevin calculation of fission in the actinide region. As a next step, we will perform a 5D Langevin calculation that includes all five parameters.

5 Acknowledgment

This work was supported by JST SPRING, Grant Number JPMJSP2150, and the Sasakawa Scientific Research Grant from the Japan Science Society. Numerical computation in this work was carried out at the Yukawa Institute Computer Facility and Cybermedia Center, Osaka University.

References

[1] T. Wada, Y. Abe and N. Carjan, Phys. Rev. Lett **70**, 3538 (1992).
[2] M. D. Usang, F. A. Ivanyuk, C. Ishizuka and S. Chiba, Phys. Rev. C **96**, 064617 (2017).
[3] V.V. Pashkevich, Nucl. Phys. A **169**, 275 (1971).
[4] N. Carjan, F. A. Ivanyuk, V. V. Pashkevich, Phys. Proc. **31**, 66 (2012).
[5] N. Carjan, F. A. Ivanyuk, Yu. Oganessian and G. Ter-Akopian, Nucl. Phys. A **942**, 97 (2015).
[6] N. Carjan, F. A. Ivanyuk and Yu. Oganessian, Nucl. Phys. A **968**, 453 (2017).
[7] N. Carjan, F. A. Ivanyuk and Yu. Oganessian, Phys. Rev. C **99**, 064606 (2019).
[8] K. T. R. Davies, A. J. Sierk and J. R. Nix, Phys. Rev. C **13**, 2385 (1976).
[9] J. Randrup and P. Moller, Phys. Rev C **88**, 064606 (2013).
[10] P. Moller, J. R. Nix, W. D. Myers and W. J. Swiatecki, Atomic Data and Nuclear data Tables **7**, 185 (1995).
[11] A.V. Ignatyuk, G.N. Smirenkin and A.S. Tishin, Sov. J. Nucl. Phys. **21**, 255 (1975).
[12] J. Tōke and W. J. Świątecki, Nucl. Phys A **372**, 141 (1981).
[13] H. Hofmann, C. Grégoire, R. Lucas and C. Ngô, Z. Phys. A **293**, 229 (1979).
[14] A. Al-Adili, D. Tarrío, K. Jansson, V. Rakopoulos, A. Solders, S. Pomp, A. Göök, F.-J. Hambsch, S. Oberstedt, and M. Vidali, Phys. Rev. C **102**, 064610 (2020).
[15] K. Shibata, O. Iwamoto, T. Nakagawa, N. Iwamoto, A. Ichihara, S. Kunieda, S. Chiba, K. Furutaka, N. Otuka, T. Ohasawa, T. Murata, H. Matsunobu, A. Zukeran, S. Kamada, and J.-i. Katakura, J. Nucl. Sci. Technol. **48**, 1 (2011).
[16] D. C. Hoffman, J. B. Wilhelmy, J. Weber, W. R. Daniels, E. K. Hulet, R. W. Lougheed, J. H. Landrum, J. F. Wild and R. J. Dupzyk, Phys. Rev. C **21**, 972, (1980).